Real-time Anterior Mitral Leaflet Tracking using Morphological Operators and Active Contours

Malik Saad Sultan[1,2], Nelson Martins[1,2,3], Eva Costa[3], Diana Veiga[3], Manuel João Ferreira[3,4],
Sandra Mattos[5] and Miguel Tavares Coimbra[1,2]

[1]*Faculdade de Ciências, Universidade do Porto, Porto, Portugal*
[2]*Instituto de Telecomunicações, Porto, Portugal*
[3]*Enermeter, Sistemas de Medição, Lda, Braga, Portugal*
[4]*Centro Algoritmi, University of Minho, Guimarães, Portugal*
[5]*Círculo do Coração de Pernambuco, Recife PE, Brazil*

Keywords: Ultrasound Images, Medical Image Processing, Active Contours, Segmentation and Tracking, Mitral Valve.

Abstract: The mitral valve plays a vital role in our circulatory system. To study its functionality, it is important to measure clinically relevant parameters, such as its thickness, mobility and shape. Since manual segmentation is impractical, time consuming and requires expert knowledge, an automatic segmentation tool can have a significant clinical impact, providing objective measures to clinicians for understanding the morphology and behaviour of the mitral valve. In this work, a real time tracking method has been proposed for ultrasound videos obtained with the Parasternal Long Axis view. The algorithm is semi-automatic, assumes manual Anterior Mitral Leaflet segmentation in the first frame and then it uses mathematical morphology algorithms to obtain tracking results, further refined by localized active contours during the whole cardiac cycle. Finally, the medial axis is extracted for a quantitative analysis. Results show that the algorithm can segment 1137 frames extracted from 9 fully annotated sequences of the real clinical video data in only 0.89 sec/frame, with an average error of 5 pixels. Furthermore, the algorithms exhibited robust tracking performance in the most difficult situations, which are large frame-to-frame displacements.

1 INTRODUCTION

1.1 Motivation

Mitral valve diseases are widespread and are commonly affected by Rheumatic Heart Disease (*RHD*) (Bisno, 2004). *RHD* is an autoimmune disease that usually begins in childhood that results from repeated episodes of acute rheumatic fever, which slowly damages the heart valves. Following one of the most relevant published studies (*WHO* and *WHF*, 2011, 2012), about 15.6 million people are affected globally from *RHD*, and require medical follow-up, being responsible for 233,000 deaths per year. Earlier detection is considered vital to control disease progression and to estimate disease burden in low-resource regions of the world (Bisno, 2004). The *RHD* thickens the Anterior Mitral Leaflet (*AML*) that results into stenosis, regurgitation, change the shape of the leaflet and shows abnormal motion patterns. Quantifying the

degree of abnormal change (morphological features) will help to identify early cases with *RHD*. Heart valve diseases create a massive economic burden on health authorities. The average surgery cost to treat mitral regurgitation was 24.871 ± 13.940 dollars per patient in Europe (Trochu, Ribeiro and Ceber, 2015, 2012, 2014). The heart valve treatments and operations are not only expensive, but also a highly risky cardiac process (Mirabel, 2007).

Echocardiography is a non-invasive, non-ionizing and comparatively low cost imaging modality that is capable of analysing fast moving valve structures in real time. It is available as portable tool and thus it is considered an appropriate choice for the diagnosis of heart diseases, especially in low-resource areas (Reményi, 2012). The Parasternal Long Axis view is the most suitable view to access the mitral valve and its structures (Figure 1). It provides the means to measure the clinically relevant parameters such as, thickness, mobility and valvular anatomy (Omran, 2010). Manual segmentation of these videos

Parasternal long axis

A

RV
AV
Septum
MV
AML
LA
LV
PML
Inferior Wall

B

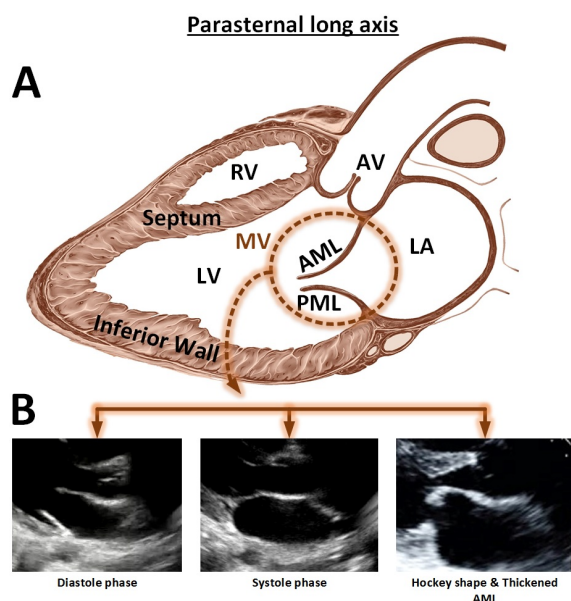Diastole phase   Systole phase   Hockey shape & Thickened AML

Figure 1: Parasternal long axis view, (A): showing Mitral valve (MV), Anterior Mitral Leaflet (AML), Posterior Mitral Leaflet (PML) and other structures. (B): Shows the MV in Diastole/Systole phase, the thickened and hockey shape leaflet.

is undesirable, given its impracticality, subjectivity and expert knowledge required. Automatic and semi-automatics methods to identify and track mitral valve structures can improve the diagnostic process, providing quick and objective measurements of clinically relevant parameters, even without any expert cardiology knowledge.

1.2 State-of-the-art in Mitral Valve Segmentation

Deformable models such as active contours were extensively used by the research community in medical image segmentation and tracking. The reason to adopt this kind of approach is their robustness against image noise and shape fragmentation, ability to track non-rigid motion and its capability to incorporate geometric constraints, such as the expected shape (Sheng, 2008). (Mikic, 1998) have proposed the use of active contours with optical flow to segment and track the *AML* in echocardiography. The algorithm fails in large frame to frame displacements, requiring user initialization in the first frame. Also, the algorithm was found computationally expensive (20 min to compute a single cardiac cycle). (Martin, 2006) have used transformation fitting with two connected active contours, optimized using dynamic programming. The algorithm requires extensive initialization and several parameters need to be tuned.

Moreover, it failed in high displacements (>10 pixels) and requires a mean processing time of about 1.8 seconds with a restricted number of iterations (10) to process a single frame. (Zhou, 2012) proposed an algorithm for mitral leaflet detection and tracking based on outlier detection in a low-rank matrix and was tested on 2D and 3D ultrasound. The algorithm was automatic and unsupervised (no initialization is required). However, the user needs to crop the original sequence, requires parameter adjustment, is very sensitive to rank and is computationally expensive. Literature review demands a real time segmentation and tracking algorithm with less user interaction and the ability to efficiently track the mitral valve when faced with large frame to frame displacements (Sheng, Mikic, Martin and Zhou, 2008, 1998, 2006, 2012).

Mathematical morphology is widely used in image processing for analysis of shapes, geometrical and topological structures. (Yun-gang, 2015) used morphological operations to roughly segment the left ventricle followed by a snakes active contours. Morphological features were efficiently used for the fast segmentation of ischemic viable, ischemic nonviable, and normal myocardium in echocardiographic images (Lascu, 2008).

1.3 Objective and Contributions

The objective of this work is to obtain robust and real-time tracking of the *AML* in ultrasound videos.

Our key contribution in this work is the novel use of combined morphological operators and active contours to address robust *AML* tracking in frames with large displacement.

The remainder of the paper is organized as follows. Section II provides the methodology adopted in this paper. In section III we report the results that demonstrate the accuracy of the proposed algorithm and finally section IV concludes the paper with a discussion on the problem, our contribution to it and the future work.

2 METHODOLOGY

In this work, the echocardiography video is split into frames and we assume perfect (manual) segmentation in the very first frame. The two successive frames are iteratively selected for the analysis. The thin regions of the successive images are extracted, followed by extracting the regions with large displacement. These regions are then merged with the segmentation result of the preceding frame and filtered, in the can-

didate region part. Regions are then classified based on their shapes and geometrical properties. The results are finally refined using localized active contours. Skeletonization and *AML* analysis is used as a post-processing step. A summary of this processing pipeline is depicted in Figure 2, and each step will now be explained in detail.
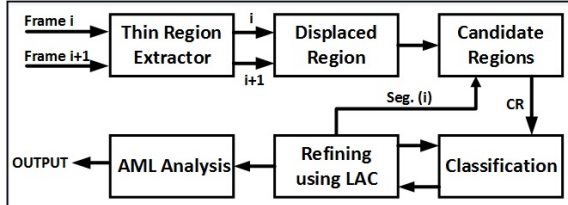

Figure 2: AML tracking pipeline.

2.1 Thin Region Extractor

In this stage, two consecutive frames were extracted iteratively until the whole cardiac cycle was covered. For the resolution of the videos used in this papers experiments the maximum recorded thickness of the *AML* was 24 pixels. Following this, all structures with width less than 24 pixels of thickness are extracted as potential regions.

The *AML* region (Figure 3C) is extracted by taking the difference between the grayscale input image (Figure 3A) and the grayscale opened image (Figure 3B) with the flat disk shape structuring element of 24 pixel diameter.
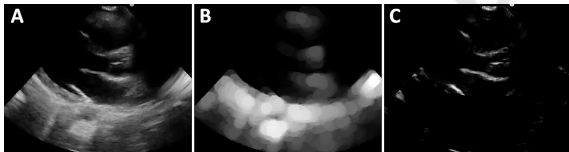

Figure 3: A) Grayscale image B) Morphological opening C) Top-hat transform.

2.2 Displaced Region

Based on the analysis of the *PLAX* videos, the thin *AML* region shows a very large displacement in successive frames compare to other regions in an image. The regions of septum, inferior wall (Figure 1) do not show significant displacement in successive frames and thus overlapped. This prior information is significant to overcome the problem of tracking in frames with large *AML* displacement.

The focus of this module is to extract region that showed large displacement from frame t-1 to frame t (Equation 1). That can simply be achieved by taking the difference of successive frames followed by

selecting only the positive intensity values (Figure 4). Hard threshold is then applied to get the binary image.

$$Disp_{gray}^t = [I_t(x,y) - I_{t-1}(x,y)] \quad Disp_{gray}^t < 0 \quad (1)$$
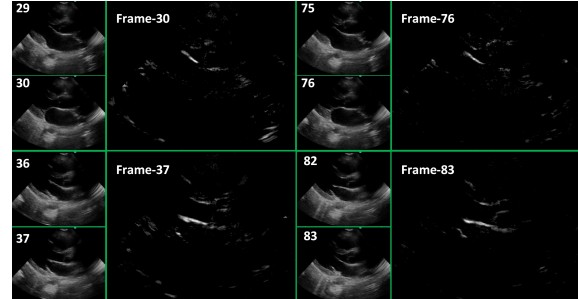

Figure 4: Regions with high displacement at four different times (frames).

2.3 Candidate Image

The segmented region obtained at the time t-1 is filtered to remove the regions which belong to the blood pool (black region) in frame at time t. Filtered region is then summed up with the results of the displaced region module. Small discontinuities (with a distance of 2 pixels or less) were merged by a morphological closing using a disk shape structuring element with a radius of 2. The obtained results are shown in Figure 5.
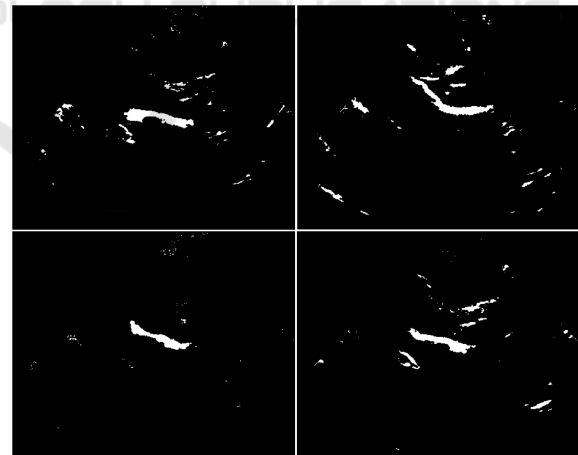

Figure 5: Candidate image for final AML classification.

2.4 Region Classification

The regions extracted from the candidate image were classified based on the morphological features, to extract the region that is most probably the *AML*. The basic morphological and geometrical features such as centroid, area, major and minor axis lengths were

used. These features are capable of providing significant structural and locality information.

These basic morphological features do not typically change significantly in successive frames. In ideal conditions, these features should be constant throughout the cardiac cycle. The features obtained from the manual segmentation in the first frame is used as a reference for the upcoming frame. After processing each frame, the reference features are automatically updated with the average, by using the feedback channel (Figure 6).
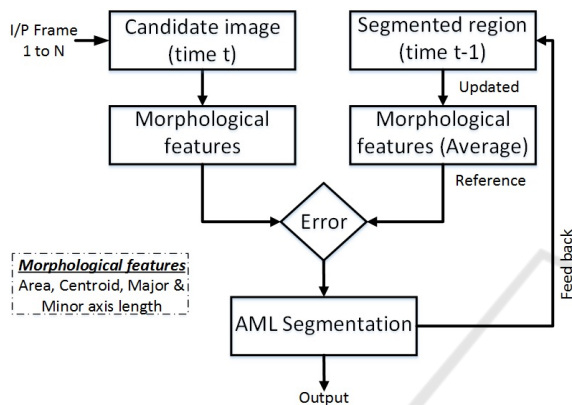

Figure 6: Classification scheme.

A relative error matrix is created that contain four vectors: centroid distance error, area error and major/minor axis length error. For evaluation purposes, the region with the minimum overall error is classified as a true positive region (*AML* region) with a good confidence and all the other regions were classified as false positive regions.

2.5 Refining using Active Contours

2.5.1 Automatic Initialization

The segmentation result of the *AML* was obtained through the morphological operators and was used as a base to initialize the active contour framework. The contour points of the initial curve are very close to the real boundaries of the *AML*. Therefore, analyzing local regions can provide robust and well defined boundaries, with a few iterations.

2.5.2 Localized Active Contour

Ultrasound images are very noisy and frequently contain heterogeneous regions, and as such neither edge based contours, nor region based contours are a suitable choice. A localized region-based active contour framework was used in this work to refine the initial contour (Lankon, 2008). This hybrid region-based

curve evolution is robust to noise and doesn't rely on the global configuration of the image.

The algorithm is based on the analysis of the local circular regions with five pixels radius, at each point on the curve. At each point the algorithm locally identifies the background and foreground optimally by their mean intensities. The formulation of the local energy function along the curve is defined as:

$$
\frac{\partial \phi}{\partial t}(x) = \delta \phi(x) \int_{\Omega_y} B(x,y) \delta \phi(y)
$$
$$
\cdot \left((I(y) - \upsilon_x)^2 - (I(y) - \mathsf{v}_x)^2 \right) dy \qquad (2)
$$
$$
+ \lambda \delta \phi(x) \, div \left(\frac{\nabla \phi(x)}{|\nabla \phi(x)|} \right)
$$

Here, is the Dirac function, $B(x,y)$ represents a region that locally defines the interior and the exterior of the region at point x and the radius of the local region is specified by the user. The uniform modelling energy is used as an internal energy (Chan, 1999). The localized version of the internal energy is defined as the local interior and exterior regions at every point on the curve. $(\upsilon_x, \mathsf{v}_x)$ are the localized version of means at each point x. The second term is the normalization term that keeps the curve smoother. It penalizes the arc length based on the weights λ tuned by the user.

2.6 AML Analysis

2.6.1 Skeletonization

The segmented *AML* region is skeletonized using morphological thinning to get a line of one pixel width. It helps to simplify the shape by preserving the topological (connectivity) characteristics. The working principle is much the same as morphological operators, requiring a binary image and a structuring element. The central pixel of the structuring element is translated to each pixel in an image. At each step, the structuring element is compared with the underlying pixels in an image. The Mark-and-Delete based templates were found very reliable and effective for thinning algorithms and thus used in this work (Zhang, 1984). The ultrasound images contain small irregularities due to speckle noise that results into unessential small branches of the skeleton. The branches need to be filtered to extract only the fundamental part. This can be achieved by discarding all those branches whose length are less than 6 pixels. The length of each branch was estimated by measuring the Euclidean distance between the branch and the end point.

2.6.2 Motion Patterns

In this part of the work, we were focused to obtain the motion pattern of the *AML*. The tracking results were analyzed to extract the important information. It was observed that the motion in the *x*-axis doesnt give any significant information. However, the motion in *y*-axis provides the base to analyze the motion of the *AML*. The mean of the y-coordinates of the obtained skeleton were saved for each frame and were plotted against time (Figure 7). The minimum and maximum peaks of the motion pattern were estimated, to classify the frame in systole and diastole phase. The pattern obtained is also useful for identifying the frames with the *AML* opened as well as closed. This information is quite useful to analyze the opening and closing of the valve. Further work can help to classify frames in early filling and late filling phase (Figure 7). This information will be helpful to identify each phase automatically. The late filling will be quite useful to extract frames in which the *AML* is perpendicular to the ultrasound beam. This is the best position to measure thickness of the *AML* tip that provides a strong clue to identify patients with a disease.
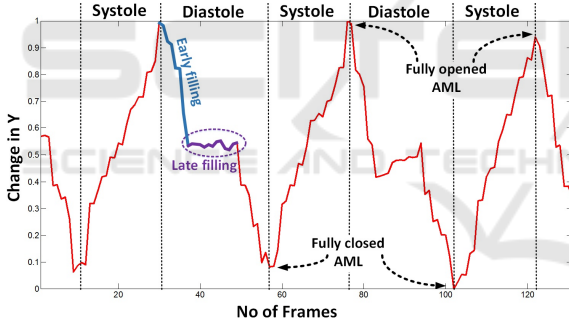

Figure 7: Motion patterns generated by AML.

2.6.3 Shape

The obtained tracking results can also be used for the shape analysis by calculating the curvature at each point on the skeleton. This can be achieved by:

$$C_{skeleton}(i) = \left\| \frac{d^2 SKL(i)}{ds^2} \right\|^2 \qquad (3)$$

The second derivative approximates the curvature of the *AML* at each point *i* on the Skeleton *SKL*. This way, we can identify the doming (hockey shape) of the *AML* in the diastolic phase, which is one of the strongest clue to identify cases with *RHD*.

3 RESULTS

3.1 Materials

A dataset of the mitral valve videos obtained from the *PLAX* view in ultrasound has been collected during the activities of Real Hospital Português, in Recife, Brazil. The videos were obtained using a M-Turbo model by SonoSite ultrasound system, with a *P*10 transducer. Nine of these exams were fully annotated by a physician using support software, to validate the proposed algorithm. These nine videos include a total of 1137 frames with the dimensions of $[351 \times 441]$.

3.2 Extended Modified Hausdorff Distance

The Modified Hausdorff Distance (Dubuisson, 1994) was proposed to obtain a distance measure to match two objects. In this work, we extended this approach by categorizing the segmented region as false positive, false negative and true positive (Equation 4). We assumed that the nearest point between Automatic Segmentation (*AS*) and Ground Truth (*GT*) with Euclidean distance smaller than 2 pixels are true positives. The part of the *AS* that is falsely segmented as *AML* were considered false positives and the parts of the *GT* that were missed by the automatic segmentation were considered as false negatives, always using 2 pixels distance as reference *T* (Figure 8).

$$d_{AS \to GT} = min\{AS, SEG\} \; FP = d > T, \; TP = d < T$$
$$d_{GT \to AS} = min\{AS, SEG\} \; FN = d > T, \; TP = d < T$$
$$D_{MHD} = max\left[avg\left(d_{AS \to GT}\right), avg\left(d_{GT \to AS}\right)\right]$$
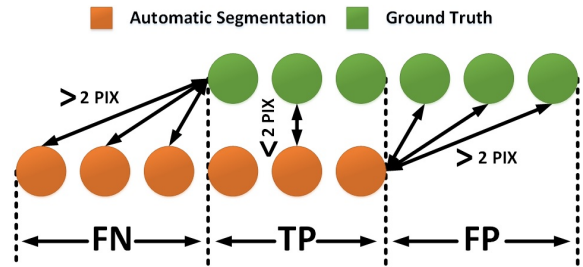$$(4)$$

Figure 8: Region classification.

3.3 Segmentation and Tracking

The algorithm has shown good computational performance and thus is suitable for the monitoring of the structures during heart procedures. Results on 2D *PLAX* ultrasound videos are presented, where the

AML was detected accurately and tracked during the whole cardiac cycle. The algorithm was robust and capable of tracking the *AML* in large displacements (around 35 pixels). The validation of the algorithm is performed by comparing the segmentation result with the physician annotation. Results were also compared with the *AML* tracking approach using active contours (Sultan, 2016).

3.3.1 Quantification

The proposed algorithm can identify the *AML* structure with an average time of 0.17 sec/frame using morphological operators and it consumes an average time of 0.67 sec/frame to refine the contour points using localized active contours. Thus, the total computational time to delineate true boundaries of the *AML* consumes 0.89 sec/frame. The reference algorithm (Sultan, 2016) takes 121 sec/frame. The algorithm was able to completely segment the structure of the *AML* with the sensitivity of 90.4% and thus the region missed by our algorithm was not very significant (average $FN = 5$ pixels). However, the main challenge faced was the regions which were falsely segmented as the part of *AML* (average $FP = 17$ pixels). This is because the *AML* and its neighbouring structures such as chordae tendineae and septum have the same texture and intensity (Figure 9).
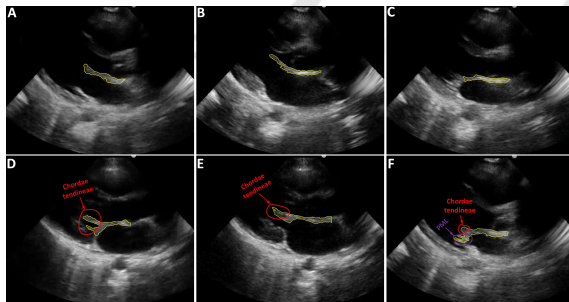

Figure 9: Visual results for the AML segmentation. (A, B, C) Shows results without outliers. (D, E, F) Shows results with outliers (fused chordae tendineae and posterior mitral leaflet (PML)).

The Table 1 show that our algorithm works equally well in all videos except 2, 7 and the *MHD* error difference between both the approaches is only 0.1 pixels. This happened because the false positive tends to increase the *MHD* error.

The first opening of the *AML* is very large. It opens sharply before the *LV* diastole (Figure 7). In the early filling, the leaflets maximally open to allow about 70 to 80% of the blood to fill the *LV*. In the ultrasound *PLAX* view this leaflet motion is very large and thus difficult to track for the present tracking

Table 1: MHD error in Pixels. (Ref.* (Sultan, 2016).

Patient No.	No. of frames	Our Approach	Ref.* Approach
1	131	5.2	5.3
2	360	6.8	4.6
3	66	4.4	5.2
4	131	4.0	4.3
5	66	5.5	5.6
6	66	5.5	5.7
7	120	5.4	4.9
8	66	4.5	4.9
9	131	3.6	3.6
Average	**1137**	**5**	**4.9**

schemes (Mikic, Martin, 1998, 2006). In the majority of the published work, researchers had used active contour frame work that requires initialization. The critical limitation of the active contours while tracking is its incapability to recover from failure. The reference algorithm (sultan, 2016) undergoes tracking failure that is overcome in this work. The proposed algorithm successfully copes with the large leaflet displacement in all videos, with the average *MHD* error of only 3.7 pixels. One can see the significant improvement from the average of 9.5 pixel error to 3.7 pixels error (Figure 10).
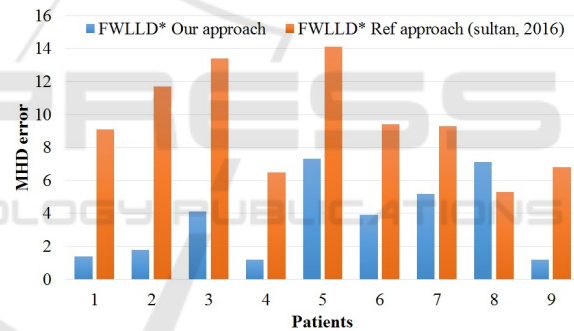

Figure 10: MHD error in Frames With Large Leaflet Displacement (FWLLD*) – In pixels.

Our algorithm outperform with respect to time consumed (difference of 1.13 minute/frame), and frame-frame displacement with the improvement of 5.8 pixels and sensitivity to noise.

4 DISCUSSION AND FUTURE WORK

In this paper, a new approach based on the morphological operators and the localized active contour is proposed. Based on the morphological operators, the algorithm finds the best match of *AML* in successive frames. It was observed that the displacement of the structures in a *PLAX* view is not significant, except the *AML* that shows the average displacement of 35 pixels in frames with fully open *AML*. The pro-

posed algorithm has successfully handled the frame-to-frame displacement of the *AML*.

A 0.89 sec/frame is still slow for a real time approach, but we believe that this value can be drastically reduced by optimizing the code, converting it to $C/C++$ and using multiple core processing.

The biggest difficulty found during the segmentation and tracking was to identify, where the *AML* starts, where it ends and the location where the chordae tendineae connects with anterior and posterior mitral leaflet. This is because all the tissues consist of elastic and collagen fibers that result into quite similar texture and intensity in ultrasound. The low quality is another obstacle that produces false positives (Figure 9).

In the future, we will focus more to improve computational time and delineate the boundaries of the *AML* correctly by filtering irrelevant regions such as chordate tendinae and posterior mitral leaflet. After having good segmentation and tracking results, we will be capable to automatically assess the functionality of the mitral valve in echocardiography.

ACKNOWLEDGEMENTS

REFERENCES

J.N. Trochu, T. L. Tourneau, J.F. Obadia, G. Caranhac, A. Beresniak, 2015. Economic burden of functional and organic mitral valve regurgitation. Archives of Cardiovascular Disease, 108, 88-96

G. S. Ribeiro, S. Y. Tartof, D. W. S. Oliveira, A. C. S. Guedes, M. G. Reis, L. W. Riley, A. I. Ko, May 2012. Surgery for Valvular Heart Disease: A Population-Based Study in a Brazilian Urban Center. PLoS One, Vol 7, issue 5

CEBR, August 2014. The economic cost of cardiovascular disease from 2014-2020 in six European economies, Centre for Economics and Business Research, London.

C. Sheng, 2008. Segmentation in echocardiographic sequences using shape-based snake model, Computing and Informatics, Vol. 27, 423435

I. Mikic, S. Krucinski, J. D. Thomas, April 1998. Segmentation and Tracking in Echocardiographic Sequences: Active Contours Guided by Optical Flow Estimates. IEEE transactions on medical imaging, vol- 17, no. 2

S. Martin, V. Daanen, O. Chavanon, J. Troccaz, 2006. Fast Segmentation of the Mitral Valve Leaflet in Echocardiography. Computer Vision Approaches to Medical Image Analysis, Vol. 4241, pp 225-235

X. Zhou, C. Yang, W. Yu, 2012. Automatic Mitral Leaflet Tracking in Echocardiography by Outlier Detection in the Low-rank Representation, IEEE Conference on Computer Vision and Pattern Recognition, IEEE Computer Society Washington, DC, USA, 972-979

M. Mirabel, B. Iung, G. Baron, D. Messika-Zeitoun, D. Dtaint, J.-L. Vanoverschelde, E. G. Butchart, P. Ravaud, A. Vahanian, 2007 .What are the characteristics of patients with severe, symptomatic, mitral regurgitation who are denied surgery?. European Heart Journal, 28, 13581365

A. Bisno, E. G. Butchart, NK Ganguly, T. Ghebrehiwet, et. al. 2004, WHO Expert Consultation on Rheumatic Fever and Rheumatic Heart Disease, Geneva

B. Remnyi, N. Wilson, A. Steer, B. Ferreira, J. Kado, K. Kumar, J. Lawrenson, G. Maguire, E. Marijon et. al. Feb 2012. World Heart Federation criteria for echocardiographic diagnosis of rheumatic heart diseasean evidence-based guideline, Nat Rev Cardiol. Vol 9, issue 5, pp 297-309

A.S. Omran, A.A. Arifi, A.A. Mohamed, 2010. Echocardiography of the mitral valve, Journal of the Saudi Heart Association, 22, 165170

L. Yun-gang, K. K. Jacky, L. Shi, Y. Guan, L. Linong, J. Qin, H. PhengAnn, C. C. Winnie, W. Defeng, 2015, Myocardial Iron Loading Assessment by Automatic Left Ventricle Segmentation with Morphological Operations and Geodesic Active Contour on T2* images, Scientific reports.

M. Lascu, D. Lascu, March 2008. A New Morphological Image Segmentation with Application in 3D Echographic Images, WSEAS Transactions on electronics, Issue 3, Vol. 5

S. Lankton, A. Tannenbaum, Nov. 2008. Localizing Region-Based Active Contours, IEEE Transactions on image processing, vol. 17, issue 11, 2029-2039

T. Chan, L. Vese, 1999. An Active Contour Model without Edges, LNCS 1682, pp. 141-151

T. Y. Zhang, C. Y. Suen, March 1984 .A Fast Parallel Algorithm for Thinning Digital Patterns, Communications of the ACM, Vol. 27, Issue 3, pp. 236-239

M. S. Sultan, N. Martins, D. Veiga, M. J. Ferreira, M. T. Coimbra, 2016. Tracking of the Anterior Mitral Leaflet in Echocardiographic Sequences using Active Contours, EMBC, 1074 1077

WHF, 2012. http://www.world-heart-federation.org /fileadmin/user_upload/documents/ Fact_sheets/2012/ RHD.pdf

WHO, 2011. World Heart Federation, World Stroke Orga-
nization, 2011. Global atlas on cardiovascular disease
prevention and control, ISBN: 9789241564373

M.-P. Dubuisson, A. K. Jain, 1994. A Modified Haus-
dorff Distance for Object Matching, Proc, interna-
tional conference on pattern recognition, Jerusalem,
Israel, pp 566-568

J. Pregowski, A. Witkowski, 2013. Percutaneous treatment
of mitral regurgitation with MitraClip device, Postep
Kardiol Inter., vol. 9, issue 4, pp. 383389